Journal of Power Sources 238 (2013) 301–312

Contents lists available at SciVerse ScienceDirect

Journal of Power Sources

journal homepage: www.elsevier.com/locate/jpowsour

A parametric study on thermal management of an air-cooled lithium-ion battery module for plug-in hybrid electric vehicles

Liwu Fan [a,1], J.M. Khodadadi [a,*], A.A. Pesaran [b]

[a] Mechanical Engineering Department, Auburn University, 1418 Wiggins Hall, Auburn, AL 36849-5341, USA
[b] National Renewable Energy Laboratory, 15013 Denver West Parkway, Golden, CO 80401-3305, USA

HIGHLIGHTS

- 3D CFD simulations were performed for an air-cooled PHEV Li-ion battery module.
- Effects of gap spacing and air flow rate were studied for trade-off concerns.
- Temperature rise can be lowered by reducing gap spacing between neighboring cells.
- Improved temperature uniformity results from a high flow rate but moderate gap spacing.
- Proposed designs featuring one-side cooling or uneven gap spacing were tested.

ARTICLE INFO

Article history:
Received 4 January 2013
Received in revised form
20 February 2013
Accepted 12 March 2013
Available online 21 March 2013

Keywords:
Thermal management
Electric vehicle
Lithium-ion battery
Air-cooled module
Temperature rise
Temperature uniformity

ABSTRACT

Three-dimensional transient thermal analyses of an air-cooled module that contains prismatic lithium-ion cells operating under an aggressive driving profile were performed using a commercial computational fluid dynamics code. The existing module utilized air cooling through evenly-spaced channels on both sides of each cell. It was found that lowering the gap spacing and/or higher flow rate of the fan lead to a decrease of the maximum temperature rise. To achieve improved temperature uniformity over the module, the gap spacing should be of a moderate size. For the given module, operating with a uniform gap spacing of 3 mm and an air flow rate of 40.8 $m^3\ h^{-1}$ appears to be the best choice that satisfies the trade-off requirements of the fan power, maximum temperature rise and temperature uniformity. Using the same gap spacing and air flow rate, a proposed design of one-side cooling is less effective than two-side cooling. Uneven gap spacing affects the temperature distributions, but it does not impact the maximum temperature rise markedly. Considering the variety of the design change options and their combinations, it is concluded that the temperature gradients along the air flow direction can be affected but are generally unavoidable.

1. Introduction

Lithium-ion batteries are the key components to power emerging electric vehicles, hybrid electric vehicles, and plug-in hybrid electric vehicles (PHEVs). Many aspects of the performance of lithium-ion battery modules are strongly affected by their operating temperature, including charge acceptance, energy capability, reliability, and so on. Some issues arising from the design of a desirable thermal management system for electric vehicle, hybrid electric vehicle, and PHEV lithium-ion battery packs were identified and addressed by Pesaran [1]. The design of thermal management systems was then improved by Vlahinos et al. [2] by using the six-sigma process. Thermal modeling and analysis of lithium-ion batteries were discussed extensively in the literature [3–7]. In order to quantitatively evaluate the influence of temperature on the performance of a battery, an advanced vehicle simulator (ADVISOR) was developed at the U.S. Department of Energy's National Renewable Energy Laboratory, which was utilized along with the commercial finite-element code ANSYS to analyze and improve existing designs of battery modules/packs [8]. Similarly, computer modeling was performed at Argonne National Laboratory to assist with the design of the thermal management systems of lithium-ion batteries [9]. Modeling effort was extended to analyze both electrochemical and thermal behaviors of lithium-ion cells [10–16]. A simple one-dimensional electrochemical and lumped thermal

* Corresponding author. Tel.: +1 334 844 3333; fax: +1 334 844 3307.
E-mail addresses: liwufan@gmail.com (L. Fan), khodajm@auburn.edu (J.M. Khodadadi).
[1] Current address: Institute of Thermal Science and Power Systems, Department of Energy Engineering, Zhejiang University, Hangzhou, Zhejiang 310027, PR China.

0378-7753/$ – see front matter © 2013 Elsevier B.V. All rights reserved.
http://dx.doi.org/10.1016/j.jpowsour.2013.03.050

Nomenclature

C_p	specific heat (J kg^{-1} K^{-1})
d	gap spacing between neighboring cells (mm)
D	diameter (m)
P	pressure (Pa)
Q	volumetric heat generation rate (W m^{-3})
Re	Reynolds number
t	time (s)
T	temperature (°C)
U	velocity (m s^{-1})
V	volumetric flow rate (m^3 h^{-1})

Greek symbols

μ	dynamic viscosity (kg m^{-1} s^{-1})
ρ	density (kg m^{-3})

Subscripts

fan	condition for the fan
gap	condition for the gap between neighboring cells
max	maximum value

model was developed by Smith and Wang [17] to study both pulse power limitations and thermal behavior of a lithium-ion hybrid electric vehicle battery pack. Kim and Pesaran [18] presented theoretical and computational comparison of the cooling effectiveness of a battery pack using different coolants, e.g., air, mineral oil and water/glycol. The advantages and disadvantages of the air-cooling system as compared to direct-contact liquid cooling were identified. More recently, it was shown numerically that the use of a reciprocating air flow is able to improve temperature uniformity of a lithium-ion battery pack [19]. Due to the simplicity of an air-cooling system, it is highly preferred in many applications. In the framework of forced-air cooling, however, there is a lack of detailed parametric studies in the literature to systematically consider the effects of geometric parameters and blower power on cooling effectiveness.

In view of this, a parametric study on the thermal management system of an air-cooled module consisting of evenly distributed prismatic lithium-ion cells was performed numerically. Critical quantities that include maximum temperature rise, temperature uniformity (as measured by the difference between cells with maximum and minimum temperatures) of the module and the required fan power were extracted from the computational results. A number of design change options, namely one-side vs. two-side, uneven vs. even gap spacing, and their combinations, were compared based on the aforementioned quantities.

2. Problem formulation

In the present investigation, analysis was focused on a PHEV air-cooled module containing lithium-ion cells being discharged/charged under an aggressive scaled power profile. To arrive at this power profile, we used the analysis by Pesaran et al. [20] for a mid-size sedan PHEV with 64 km (40 miles) all-electric range driving over a standard driving test profile by Environmental Protection Agency called US06 [21]. This drive cycle is 600 s (10 min) with an average speed of 77.5 km h^{-1} and is considered aggressive compared to other drive cycles. Power profile from the battery pack of the PHEV 40 was scaled to the module and then increased by 30% to make it a higher power unit to generate more heat. The power profile will be called 1.3 × US06 (PHEV40) here on.

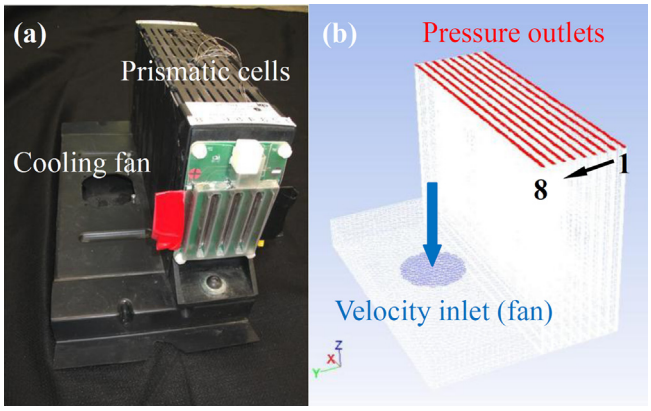

Fig. 1. A PHEV air-cooled module: (a) photograph of the existing module (courtesy of John Ireland of the U.S. Department of Energy's National Renewable Energy Laboratory), and (b) simplified computational domain with boundary conditions.

The module is shown in Fig. 1a and contains eight 15 Ah lithium-ion prismatic pouch cells with manganese oxide cathode, graphite anode, and standard combination of linear and cyclic alkyl carbonates with $LiPF_6$ salt. However, the thermal modeling approach discussed in this paper could be applied to any battery chemistry. The eight 15-Ah prismatic cells were positioned vertically inside the module with evenly spaced gaps between neighboring cells. A cooling fan positioned on the side of the module can be turned on to assist in lowering the operating temperatures. The cells were numbered 1 to 8, with 8 denoting the cell closest to the fan, as shown in Fig. 1b. The air flow can be redirected by the manifold configuration of the module and flow through the nine individual gaps between cells; the air stream then leaves the module at the nine outlet ports on top of the module, which are exposed to the atmosphere. For simplicity, the tabs of the cells and all other electronic components are excluded in the model. The fan was modeled by imposing a constant velocity boundary condition at the inlet (circle), whereas the outlets (nine stripes) were specified as pressure outlet boundary conditions (see Fig. 1b). The adiabatic, no-slip wall boundary condition was applied to all other boundaries (white walls) of the computational domain.

The dimensions of the prismatic cells were measured and the thermophysical properties for a commercial 15-Ah cell were used for this modeling effort. In addition, the heat generation rate for the commercial cell under the 1.3 × US06 (PHEV 40) power profile testing was measured using the National Renewable Energy Laboratory's isothermal calorimeter. The dimensions and thermophysical properties of the prismatic cells are listed in Table 1. The module was assumed to be operated under the 1.3 × US06 (PHEV 40) power profile for 600 s, during which the time-averaged heat generation rate was applied. The actual gap spacing between the neighboring cells (d) in the existing module was equal to 3 mm. The imposed air velocity at the inlet port was determined via the volumetric flow rate (V) of the fan, which was equal to 20.4 m^3 h^{-1}.

Table 1
Dimensions and properties of the prismatic cells used in the model.

Dimension or property	Value
Active area dimensions (mm)	6 × 145 × 255 (tabs excluded)
Density (kg m^{-3})	~2335
Specific heat capacity (J kg^{-1} K^{-1})	~745
Thermal conductivity (W m^{-1} K^{-1})	~27 (along surfaces) ~0.8 (in thickness direction)
Heat generation rate (W m^{-3})	28,000 (1.3 × US06, PHEV 40)

The ambient temperature, which is also the initial temperature of the entire module, assumed to be about 27 °C. In this modeling effort, thermal radiation transfer was assumed to be negligible and was not taken into account.

3. Numerical solution

During the past three decades, design, analysis, and optimization of equipment and/or processes involving fluid flow have extensively been performed by using computational fluid dynamics techniques and codes. In this numerical study, ANSYS Fluent 12.0 was utilized. The meshed computational domain with boundary conditions is shown in Fig. 1b. After testing several grid densities, an appropriate grid system of about 100,000 hexahedral cells over the entire computational domain was used. The time step for integrating the governing equations was set to be 1 s after testing dependence of time step on the solution. The convergence criterion was set such that the residuals of the governing equations for flow and thermal energy were below 10^{-4} and 10^{-6}, respectively.

Each of the eight cells in this problem can be considered as a vertically oriented homogeneous block with an internal heat source experiencing forced convection on both sides. The lumped maximum temperature rise in case of "no forced air cooling" for each cell after 600 s was estimated to be about 9.66 °C using a transient lumped model, as given by:

$$\Delta T_{\max} = \frac{Q}{\rho C_p}\Delta t, \tag{1}$$

This can be viewed as an ideal upper limit for the temperature rise of an individual cell. The predicted temperature rises will be expected to be lower than this value due to the heat extraction from the individual prismatic cell by passive air cooling. It is noted that this theoretical maximum temperature rise was verified by a preliminary thermal imaging test on the 15-Ah cells being operated under the 1.3 × US06 (PHEV 40) power profile testing. As a good agreement was obtained between the thermal imaging and numerical simulation results of the cells, the code and physical model with appropriate parameters were then used for all the simulations.

The Reynolds number through the fan (Re_{fan}) corresponding to a flow rate of 20.4 m^3 h^{-1} was determined to be approximately 8×10^3, indicating that the cooling air entering the module was in the turbulent regime. A two-equation high-Reynolds number turbulence model ($k-\varepsilon$) was utilized. Assuming equal division of the cooling air into each of the individual gaps, for a flow rate of 20.4 m^3 h^{-1} through the fan the Reynolds number of the flow within each gap (25.5 cm long) was determined to be approximately 338, indicating that the cooling air entering each gap was in the laminar regime. Of course, in the actual module, the distribution of flow rate among the channels is not uniform due to asymmetry of the location of the fan to the air passages for each cell. The ANSYS Fluent simulations account for the proximity of the fan to each air gap; thus, the flow rate and associated Reynolds number will be different for each passage. We anticipate the flow to be laminar in each of the air passages as the Reynolds number would still be below 1000.

A parametric study was undertaken to investigate the effects of:

1. variations of the gap spacing and the air flow rate of the fan,
2. one-side cooling scheme, and
3. uneven gap spacing scheme.

These various design options were then compared based on the observed temperature rise, uniformity of the temperature fields and the required power of the fan.

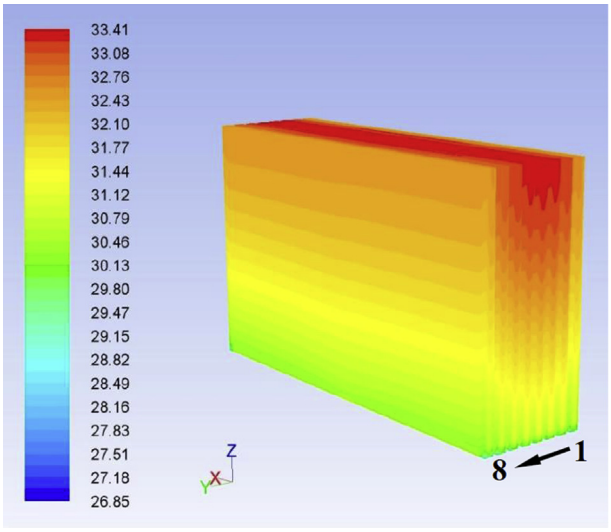

Fig. 2. Three-dimensional temperature distribution (unit: °C) of the cells after 600 s for the case of $d = 3$ mm and $V = 20.4$ m^3 h^{-1}.

4. Results and discussion

For the present case that corresponds to the operation of the existing module ($d = 3$ mm and $V = 20.4$ m^3 h^{-1}), the predicted three-dimensional temperature distributions within the eight cells at the end of discharge operation ($t = 600$ s) are shown in Fig. 2. The maximum temperature rise within the eight cells is approximately 6.53 °C, which was found at the top of cell #4. As compared to the lumped temperature rise for the case of "no forced cooling," the maximum temperature rise was lower by about 3 °C upon using forced air cooling. The temperature fields are horizontally stratified over each cell, as shown by the nearly horizontal isotherms. To quantitatively compare the predicted temperature field information cell by cell, the maximum, minimum, and average temperature rise values within each cell are listed in Table 2, in which the standard deviations of the temperature distribution was also calculated to represent the temperature uniformity within each cell. The middle cells, which exhibit the highest maximum temperature rises near their top regions, also have the poorest temperature uniformity, as evidenced by the high value of the standard deviation. One can denote the difference between the predicted maximum and minimum temperature rise within each cell as the "temperature gradient" within that cell. This quantity is critical to the design and optimization of thermal management systems for batteries since the uniformity of the temperature field directly affects the battery life. The two side cells (#1 and #8) have temperature gradients of about 2.4 °C, whereas the temperature gradient is nearly 3 °C for the middle cells.

Table 2
Values of the maximum, minimum and average temperature rises, the temperature difference (defined as maximum minus minimum) and the standard deviations of the temperature fields within each cell after 600 s for the case of $d = 3$ mm and $V = 20.4$ m^3 h^{-1}.

Quantity	Corresponding cell temperature rise (unit: °C)							
	#1	#2	#3	#4	#5	#6	#7	#8
Maximum	5.84	6.38	6.50	6.53	6.51	6.43	6.26	5.77
Minimum	3.55	3.76	3.80	3.79	3.73	3.62	3.48	3.32
Average	4.89	5.33	5.43	5.46	5.43	5.33	5.16	4.79
Difference	2.29	2.62	2.70	2.74	2.78	2.81	2.78	2.45
St. dev.	0.681	0.802	0.812	0.811	0.819	0.825	0.816	0.720

4.1. Effects of gap spacing between neighboring cells

By fixing the fan's supply flow rate at $V = 20.4\ m^3\ h^{-1}$, the effects of the gap spacing (d) on the predictions of the temperature fields were parametrically investigated. The gap spacing value was either increased ($d = 4$ or 5 mm) or reduced ($d = 1$ or 2 mm). Note that this variation in the gap spacing did not affect the value of the Reynolds number in the gap that was set at 338, so the flow was laminar. Using the same temperature scale, the predicted three-dimensional temperature distributions within the cells after 600 s are compared in Fig. 3 for five gap spacing values, including the original case of $d = 3$ mm, with the temperature scale set between 26.85 °C and 36.50 °C. The lower limit is the uniform initial temperature of the module, and the upper limit corresponds to the maximum temperature rise for the case of "no forced cooling" (about 9.65 °C). Obviously, with the aid of the cooling air provided by the fan, the observed temperatures for different gap spacing values never attain the high temperature of the red region of the temperature scale. With a smaller gap spacing, higher temperatures are observed in the middle of the module; as the gap spacing is increased, the hottest position migrates toward cell #8, which is closest to the fan. Because natural convection does not play any significant role in cooling the individual cells, this suggests that the flow and thus the Reynolds numbers within the individual gaps are non-uniform and different from the ideal case of 338, i.e., based on the more effective cooling of the cell farthest from to the fan (#1), the prevailing Reynolds numbers within the two gaps on either side of cell #1 are greater that the corresponding values in the two gaps on either side of cell #8. This will be presented quantitatively below. In order to provide guidance into optimization of this module, the behavior of the temperature uniformity over each cell is a critical quantity. Standard deviations of the temperature fields within the cells are a measure of the temperature uniformity. These values are listed in Table 3, in which the standard deviation values in the "overall" column are the values obtained considering all the cells and their associated temperature fields. In general, by fixing the fan's flow rate, the maximum temperature rise was consistently increased (due to higher heat transfer rates), but the overall temperature uniformity of each cell was promoted as the gap spacing was increased and vice versa. Varying the gap spacing from $d = 1$ mm to $d = 5$ mm, the maximum temperature rise within the eight cells was increased by about 0.77 °C, with a simultaneous favorable compensation that the temperature uniformity was improved by 0.41 °C (far right column of Table 3). Among the eight cells, the side cells exhibited improved temperature uniformity compared to those in the middle of the module as the separation distance of the gap was increased. Similar to the discussion above in relation to the effective cooling of the cell farthest from to the fan (#1) due to increased flow rate of the cooling air, an improved temperature uniformity of the side cells is also achieved.

Having discussed the general observations in relation to dependence of the thermal fields on the gap spacing for a constant flow rate of the air blower, we now consider results for a parametric study of the various cooling air flow rates for a given gap spacing.

4.2. Effects of the fan's flow rate

The gap spacing was fixed at its original value of $d = 3$ mm, and the effects of the fan's flow rate were examined. The flow rate of the cooling air was either increased (V = 30.6 or 40.8 $m^3\ h^{-1}$) or reduced (10.2 $m^3\ h^{-1}$). The corresponding values of the gap Reynolds numbers if the flow was divided evenly among the nine gaps were 507, 676 and 169, respectively. Note that $V = 0\ m^3\ h^{-1}$ corresponds to the case of "no forced cooling." The predicted three-dimensional temperature distributions within the cells after 600 s for the various air flow rates are compared in Fig. 4, in which the temperature scales are the same as those in Fig. 3. It is observed that increasing the blower's flow rate significantly lowers the temperature rise within the module. For example, for the case of $V = 40.8\ m^3\ h^{-1}$, the temperature contours within the module fall into the green and blue regions of the temperature scale. Compared to the original case of $V = 20.4\ m^3\ h^{-1}$, doubling the air flow rate reduces the maximum temperature rise by about 1.8 °C. Whereas for the least value of the air flow rate higher temperatures are observed in the middle of the module, as the air flow rate is raised the hottest position migrates toward cell #8, which is closest to the fan. Because natural convection is negligible, this suggests that the Reynolds numbers within the individual gaps are different than their respective even-dividing values given earlier. In other words, with the more effective cooling of the cell farthest from to the fan (cell #1), the Reynolds numbers within the two gaps surrounding cell #1 are greater that the corresponding values in the two gaps

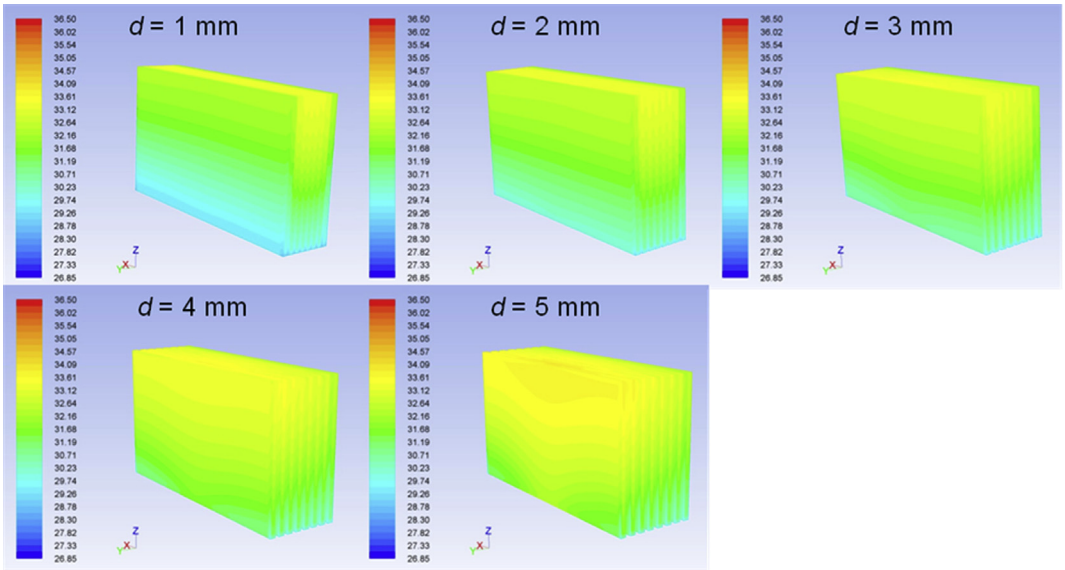

Fig. 3. Three-dimensional temperature distributions (unit: °C) in the cells after 600 s for various gap spacing values at $V = 20.4\ m^3\ h^{-1}$.

Table 3
Standard deviations of the temperature fields (unit: °C) within the cells for various gap spacing values for $V = 20.4$ m^3 h^{-1}.

Gap spacing (mm)	#1	#2	#3	#4	#5	#6	#7	#8	Overall
1	0.968	1.096	1.137	1.144	1.145	1.138	1.099	1.002	1.135
2	0.780	0.938	0.961	0.965	0.967	0.968	0.953	0.826	0.953
3	0.681	0.802	0.812	0.811	0.819	0.825	0.816	0.720	0.823
4	0.629	0.743	0.760	0.765	0.771	0.779	0.782	0.694	0.782
5	0.550	0.637	0.656	0.670	0.683	0.694	0.701	0.635	0.720

surrounding cell #8. This phenomenon is similar to what was observed above when the gap distance was varied for a constant air flow rate. This will be discussed quantitatively below.

As the air flow rate varied from 10.2 to 40.8 m^3 h^{-1}, the maximum temperature rise within the eight cells was lowered by about 3.27 °C, with a simultaneous favorable compensation that the temperature uniformity was improved by 0.2 °C (far right column of Table 4, where the values of the standard deviations of the temperature fields within the cells for various flow rates and $d = 3$ mm are given). However, the consistent improvement in temperature uniformity that is linked to the rise of the air flow rate is not equally featured by the various cells. For example, the cell that is located farthest from the blower (cell #1) always has the most uniform temperature. The reasoning behind this observation was presented in preceding discussion.

4.3. Dependence of the Reynolds number in each gap on the gap distance and air flow rate

Throughout the course of the parametric study, five different gap spacing values ($d = 1$, 2, 3, 4, and 5 mm) and four fan flow rates ($V = 10.2$, 20.4, 30.6, and 40.8 m^3 h^{-1}) were studied. Eight out of the 20 combinations were discussed in great detail above. The observed maximum temperature rise and the extent of the temperature uniformity were dependent on the gap spacing and the air flow rate. Based on the observed temperature fields discussed earlier, the two gaps on the side of cell #1 that is the farthest from the fan consistently were the channels that provided enhanced cooling as the gap spacing or air flow rate was raised. This was speculated to be linked to uneven division of the cooling air among the various gaps. Data will be presented to substantiate our hypothesis that the flow rate and correspondingly, the Reynolds numbers are varied among the nine gaps. Two of the 20 cases were selected based on the criterion associated with the theory of laminar flow within a channel bounded by two parallel infinitely long plates. According to the theory, the hydrodynamic entrance length, which is the length needed for a perfectly uniform velocity profile to transform to a fully developed parabolic distribution is a linear function of the Reynolds number. Based on this, the two extreme cases ($d = 1$ mm and $V = 10.2$ m^3 h^{-1}) and ($d = 5$ mm and $V = 40.8$ m^3 h^{-1}) were selected. For the case of $d = 1$ mm and $V = 10.2$ m^3 h^{-1}, the flow within the gap develops very quickly and remains fully developed before leaving the module. For the other extreme case, that is, $d = 5$ mm and $V = 40.8$ m^3 h^{-1}, the flow never attains the fully developed state.

The predicted velocity profiles in three of the nine channels at different heights along the central plane of the module are plotted in Fig. 5 for the case of $d = 1$ mm and $V = 10.2$ m^3 h^{-1}. The channels are numbered in the same manner for the prismatic cells so that the #1 gap is the farthest away from the cooling fan. Note that at the entrance to each channel, there is little distinction among the velocity profiles, suggesting that the air flow originating from the fan has been distributed rather evenly among the nine gaps. Justification for this statement is given in Table 5, where the predicted mass flow rates at the exit planes of the individual channels are listed. The computed flow rates are nearly identical, and the flow rates in the two side gaps differ from an ideal value of approximately 1.13 m^3 h^{-1} by no more than 2.8%. Due to the short hydrodynamic

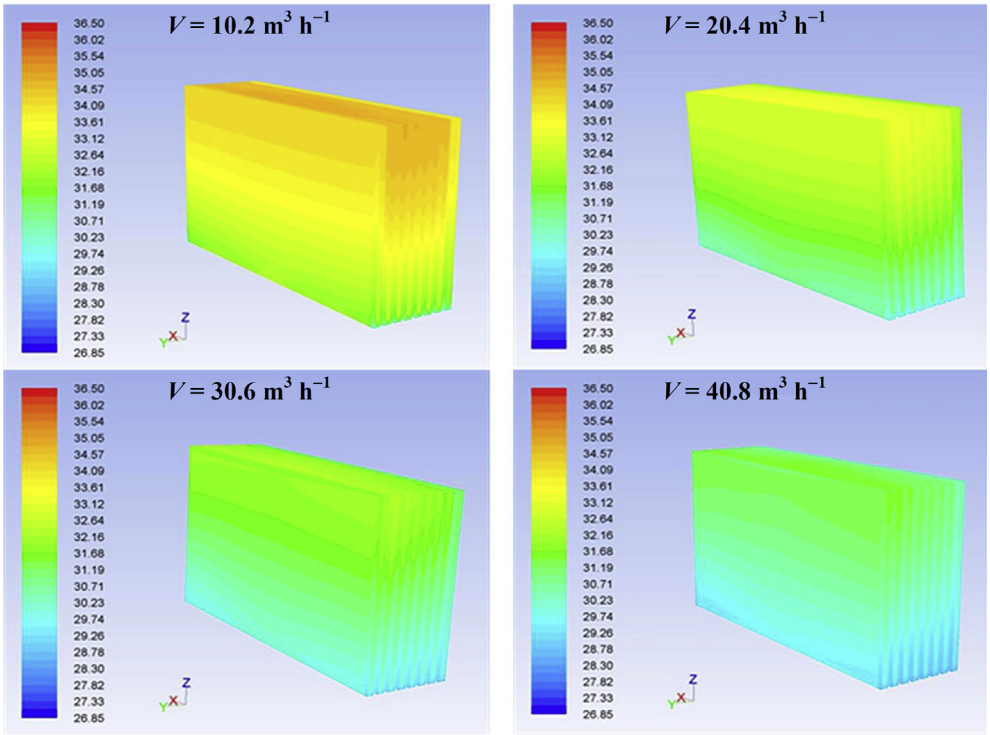

Fig. 4. Three-dimensional temperature distributions (unit: °C) in the cells after 600 s for various flow rates of the fan for $d = 3$ mm.

Table 4
Standard deviations of the temperature fields (unit: °C) within the cells for various flow rates of the cooling fan for $d = 3$ mm.

Flow rate ($m^3\ h^{-1}$)	#1	#2	#3	#4	#5	#6	#7	#8	Overall
10.2	0.747	0.836	0.846	0.845	0.843	0.842	0.830	0.765	0.863
20.4	0.681	0.802	0.812	0.811	0.819	0.825	0.816	0.720	0.823
30.6	0.568	0.707	0.736	0.749	0.760	0.771	0.779	0.690	0.756
40.8	0.489	0.611	0.641	0.654	0.665	0.676	0.686	0.619	0.665

development lengths for this case (approximate Reynolds number of 169 in each channel), the velocity profiles at the mid-plane and the exit of the individual gaps are indistinguishable and their peak values are reached halfway between the two sides, as expected for fully developed laminar channel flow. Such a repetitive duplication of the flow fields in each neighboring gap will in turn give rise to the establishment of the relatively hotter inner zone that was observed in the middle of the pack of the cells. A representative temperature distribution under this condition was already observed in Fig. 3 with $d = 1$ mm.

In contrast to the case of the smallest gap spacing and flow rate (presented in Fig. 5), for the case with the highest gap spacing and air flow ($d = 5$ mm and $V = 40.8\ m^3\ h^{-1}$), the fluid within each channel is not able to achieve the fully developed status before leaving the module. The predicted velocity profiles in three of the nine channels at different heights along the central plane of the module for this case are plotted in Fig. 6. Note that there are distinct differences among the profiles and the magnitudes of the velocity at the entrance to each channel. These skewed velocity profiles and their magnitudes indicate that the air flow originating from the fan was distributed unevenly among the nine gaps. Compared to gaps #5 and #9, which feature almost identical inlet plane profiles, the velocity distribution at the inlet plane of gap #1 suggests that more fluid was drawn into this gap, which is located farthest from the fan. The computed flow rates within the individual channels for the case of Fig. 6 (second row of Table 5) differ greatly from each other with each gap receiving more cooling air than the neighboring gap that was closer to the fan. Thus, it is observed that the flow rate in gap #1 is about four times that of the flow rate in gap #9. This uneven distribution of the cooling air was also reflected in the actual values of the Reynolds number within these nine gaps (an estimated range of 300 to 1100).

Due to the long hydrodynamic development lengths needed for this case, which happened to be longer that the length of the channels (0.145 m), the velocity profiles at the mid-plane and exit stations of the individual gaps did not coincide. Even though the velocity profiles showed peak values at the mid-plane and exit stations, they cannot be considered to be fully developed laminar channel flow. Such an uneven variation in air flow rates among the gaps will give rise to the establishment of non-uniform cooling within the module. The cells farthest from the fan are cooled more effectively compared to the cells that are closest to the fan but were deprived from an appropriate flow supply. Representative temperature distributions under similar conditions can be observed in Figs. 3 and 4. It should be mentioned that establishment of secondary flow structures with vortex-like path lines on horizontal planes are expected to be present in the existing design. Due to the negligible role of natural convection, the temperature distributions within each cell exhibited deviations from horizontal contour patterns. Such temperature distributions under similar conditions can be observed in Figs. 3 and 4. In general, based on the results presented in Table 5, it is suggested that with shorter gap spacings and/or lower fan flow rates, the distribution of cooling air within the gaps tends to be more uniform. The uneven distribution of the flow rates appears to have a stronger dependence on the gap spacing.

Having discussed representative behavior of the maximum temperature rise and temperature uniformity of the module in relation to the gap spacing, flow rate of the fan and the uneven distribution of the cooling air within the nine gaps, we now present all the results for the parametric study of the existing design.

4.4. Combined gap spacing and air flow effects on the given design

The five different gap spacing values ($d = 1$, 2, 3, 4, and 5 mm) and four flow rates of the fan ($V = 10.2$, 20.4, 30.6, and 40.8 $m^3\ h^{-1}$) lead to a total of 20 combinations. Eight of these cases were discussed in great detail above. The effects of the gap spacing and the flow rate of the fan on the maximum temperature rise and temperature uniformity over the entire module are shown in Fig. 7. Essentially, for each of the 20 combinations, the maximum temperature rise among the eight cells and the standard deviations of the temperature fields of the eight cells combined were computed and are shown in Fig. 7. Considering the computed results in Fig. 7a, if a thermal designer plans to achieve low temperature rise within the module, a higher flow rate of the fan is always favorable and using narrower gap spacing could generally be helpful. However, it is observed that a narrow gap spacing and a high flow rate of the fan could potentially lead to poor temperature uniformity over the entire module (Fig. 7b). One the other hand, if temperature uniformity is the main criterion for the selection of one gap spacing/fan flow rate combination, the higher flow rate but a moderate gap spacing is the correct choice. Trade-off issues between maximum temperature rise and temperature uniformity need to be considered in making the final selection. It should be emphasized that the temperature rise values and the uniformity parameter shown in Fig. 7 are for the entire module rather than individual cells. The values of the maximum temperature rise and standard deviations of the temperature fields within individual cells are compared for the 20 cases in Fig. 8. A flat line corresponding to the temperature rise of 9.65 °C is also given in Fig. 8a, as the baseline case of "no forced cooling." For a majority of the combinations, the two side

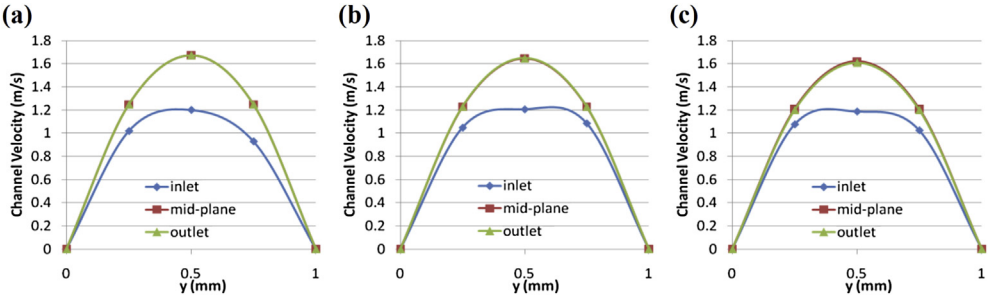

Fig. 5. The predicted velocity profiles in the (a) #1, (b) #5, and (c) #9 gaps at different positions in the vertical direction for the case of $d = 1$ mm and $V = 10.2\ m^3\ h^{-1}$.

Table 5
Mass flow rates (unit: g s^{-1}) in the individual gaps for four combinations that are (A) $d = 1$ mm and $V = 10.2$ m^3 h^{-1}, (B) $d = 5$ mm and $V = 40.8$ m^3 h^{-1}, (C) $d = 1$ mm and $V = 40.8$ m^3 h^{-1}, and (D) $d = 5$ mm and $V = 10.2$ m^3 h^{-1}.

No.	Mass flow rate in each air gap								
	#1	#2	#3	#4	#5	#6	#7	#8	#9
A	0.389	0.387	0.386	0.386	0.384	0.384	0.384	0.384	0.373
B	2.451	2.057	1.810	1.651	1.504	1.378	1.246	1.048	0.673
C	0.164	0.156	0.152	0.152	0.1523	0.152	0.152	0.152	0.150
D	0.489	0.451	0.421	0.400	0.381	0.365	0.349	0.331	0.270

cells always exhibit the lowest temperature rises and best temperature uniformities compared to the remaining six cells. For a constant air flow rate and lower gap spacing values, the curves shown in Fig. 8 are nearly symmetric about the middle gap position. This can be related to the nearly even distribution of the cooling air within each of the nine gaps, as observed in Fig. 5 and Table 5. As the gap spacing is increased for a constant flow rate, the maximum temperature rise values diminish. The values of the standard deviation are also lowered as the gap spacing is increased and the relative symmetry of the curves about the middle gap is broken. As discussed earlier, this indicates that in spite of a constant air supply, cooling within individual channels becomes more uneven and the farthest cell from the fan (cell #1) exhibits the lowest temperature rise within the module and also possesses the most uniform temperature distribution.

4.5. Fan power requirements

The ideal fan power, which is evaluated as the product of the pressure drop and the volumetric flow rate generated by the cooling fan, was calculated using the CFD results. The equation is given by

$$\text{Power} = \Delta P \times V \tag{2}$$

where ΔP is the pressure drop across the cooling fan. The predicted "ideal" fan power values for the 20 combinations are drawn in Fig. 9, in which a semi-log graph is utilized. The "actual" fan power is the "ideal" fan power divided by the efficiency of the fan/motor. The ideal (and the actual) required fan power is consistently lower if the gap spacing is raised while keeping the air flow rate unchanged. For a given gap spacing, the required fan power is raised as the flow rate of the fan is increased. Comparing the opposite trends of fan power and the maximum temperature rise within the module (Fig. 7a), the thermal designer has to decide on a trade-off between the maximum temperature rise that can be tolerated at the expense of a fan with a greater throughput. Considering the trade-off among maximum temperature rise, temperature uniformity and the power of the fan, the case of $d = 3$ mm and $V = 40.8$ m^3 h^{-1} appears to be the best choice for the current two-side cooling arrangement.

Having discussed results of a parametric study of 20 cases combining variations of gap spacing and air flow rate of the fan

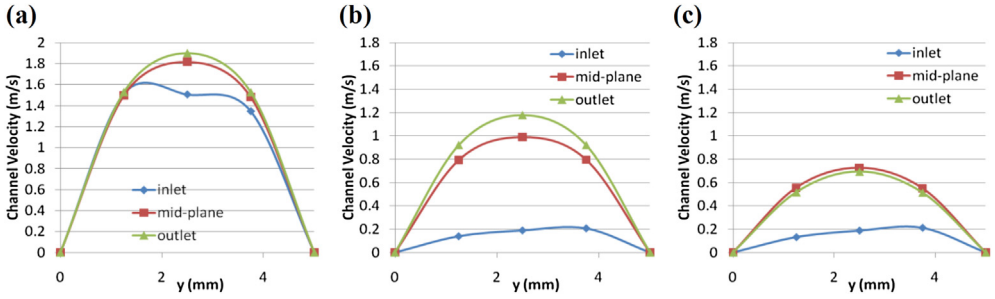

Fig. 6. The predicted velocity profiles in the (a) #1, (b) #5, and (c) #9 gaps at different positions in the vertical direction for the case of $d = 5$ mm and $V = 40.8$ m^3 h^{-1}.

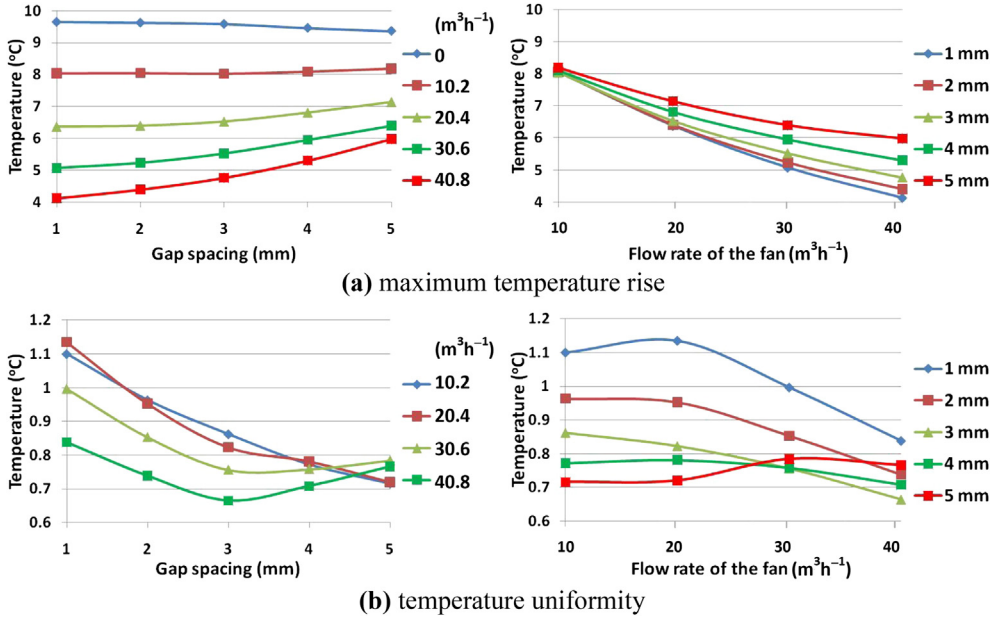

Fig. 7. The effects of gap spacing and flow rate of the fan on the (a) maximum temperature rise and (b) temperature uniformity of the entire module for 20 combinations.

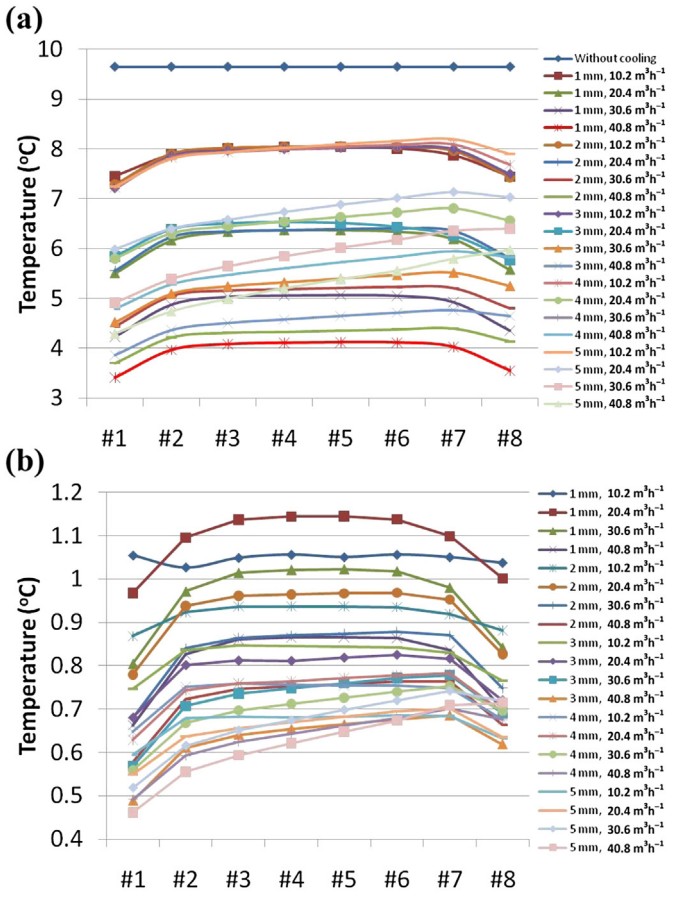

Fig. 8. The values of the (a) maximum temperature rise and (b) standard deviations of the temperature distribution within the individual cells for 20 combinations of various values of gap spacing and flow rate of the fan.

with two-side cooling of each individual cell, the investigation was then focused on exploring proposed designs to quantify the influence of:

1. a one-side cooling scheme, and
2. uneven gap spacing.

4.6. Proposed design no. 1: one-side cooling of each cell

The existing design of the module that was investigated above is a two-side cooling approach because the cooling air stream flows over both sides of the individual cells, as shown in Fig. 10a. Pairs of neighboring cells may be grouped together to give a proposed design of a one-side cooling scheme such that the air stream only flows over one side of each pair of cells. As shown in Fig. 10b, this proposed design could lead to a more compact module. Taking the gap spacing for both designs to be equal to d, the proposed design will be thinner than the original one by a thickness of $4d$. In practice, a non-conductive thin separator may be placed in the middle of each pair of cells (the black line shown in Fig. 10b). In the CFD model, the pairs of neighboring cells were assumed to be in direct contact and the interface between them was modeled as an insulated wall. With the proposed gap spacing kept the same as the original design ($d = 3$ mm), the thickness of the proposed module was decreased by 12 mm. Using the same air flow rate of $V = 20.4$ m^3 h^{-1}, the predicted three-dimensional temperature distributions within the cells after 600 s for the proposed design are compared to those for the original design in Fig. 11.

Note that the temperature scales in the two figures are a bit different. With the aid of the high values of the temperature scales in Fig. 11, the maximum temperature rise within the cells is observed to have increased by nearly 0.5 °C for the proposed design. Considering the more compact volume of the module in the proposed design, the trade-off for an increase of the maximum temperature rise could be acceptable. For the same gap spacing and flow rate, as far as the maximum temperature is concerned, one-side cooling is inferior to two-side cooling, although the savings in space and lower fan power might justify its adoption. In addition, the observed temperature distributions becoming more uniform for the proposed design provide an extra advantage for adopting a one-sided cooling scheme.

A parametric study of the gap spacing with the proposed one-side cooling was performed at this stage. The predicted three-dimensional temperature distributions within the cells after 600 s for various gap spacing values are compared in Fig. 12 using the same temperature scale. It is observed that the maximum temperature rise within the cells was slightly increased with increasing gap spacing, which is consistent with the trends observed for the original two-side cooling design (Fig. 3). Similar to observations for the two-side cooling scheme, higher temperatures are observed in the middle of the module with shorter gap spacing. However, as the gap spacing is increased, the hottest position migrates toward cell 8, which is closest to the fan. The temperature uniformity was improved as the gap spacing was broadened. These trends are directly linked to the prevailing values of the Reynolds numbers within the two gaps surrounding cells #1 and #2 being greater that the corresponding values in the two gaps that surround cell #7 and #8. If volume constraints are not applied, trade-off

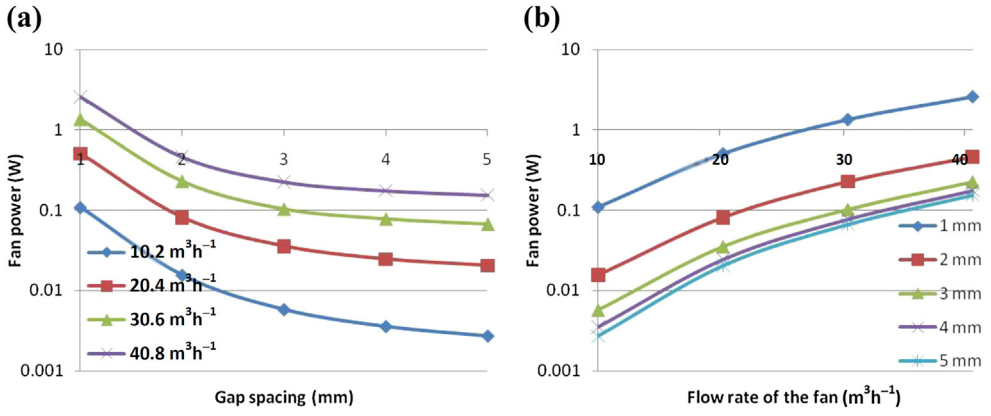

Fig. 9. The effects of (a) gap spacing and (b) flow rate on the fan power for the 20 combinations.

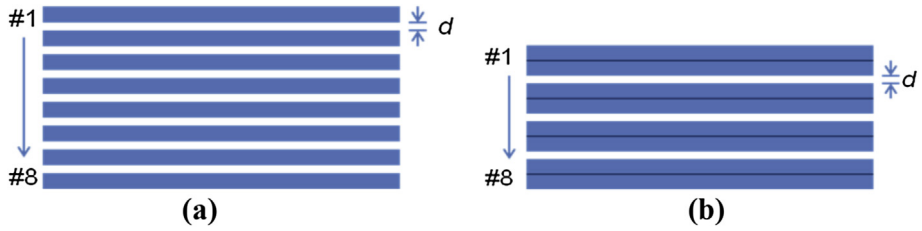

Fig. 10. Schematic diagrams of the (a) existing design of two-side cooling and the (b) proposed design with each cell cooled only from one side.

between the one-side and two-side cooling schemes should be explored. For a fixed number of identical cells, if the volume of the module is unchanged, the gap spacing for the one-side cooling design will be wider than for the two-side cooling option. For instance, since the thickness of each of the eight cells is 6 mm, a gap spacing of $d = 2$ mm for the one-side cooling design gives a nearly equal volume compared to the two-side cooling design with $d = 1$ mm. Operating with an air flow rate of $V = 20.4\ m^3\ h^{-1}$, the predicted maximum temperature rises and standard deviation of the temperature fields of the cells for these two cases are compared in Fig. 13.

As observed in Fig. 13a, with the volumes of the modules nearly identical, the module using the one-side cooling scheme exhibits slightly higher temperature rises for each cell, but the overall temperature uniformity of the module has improved (Fig. 10b). Similar trends were observed by comparing the one-side and two-side cooling options with $d = 5$ and $d = 3$ mm, which also featured nearly identical volumes. Essentially, the influence of the gap spacing on the maximum temperature rise and temperature uniformity for this proposed design was shown to be similar to the trends observed for the original design. However, the non-uniformity of the temperature field among the cells still persists,

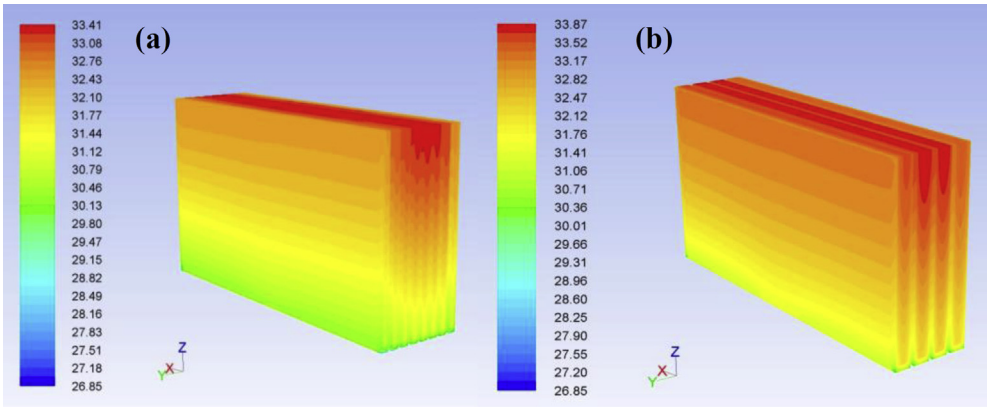

Fig. 11. Three-dimensional temperature distributions (unit: °C) within the cells after 600 s for the (a) original two-side cooling and the (b) proposed one-side cooling design with $d = 3$ mm and $V = 20.4\ m^3\ h^{-1}$.

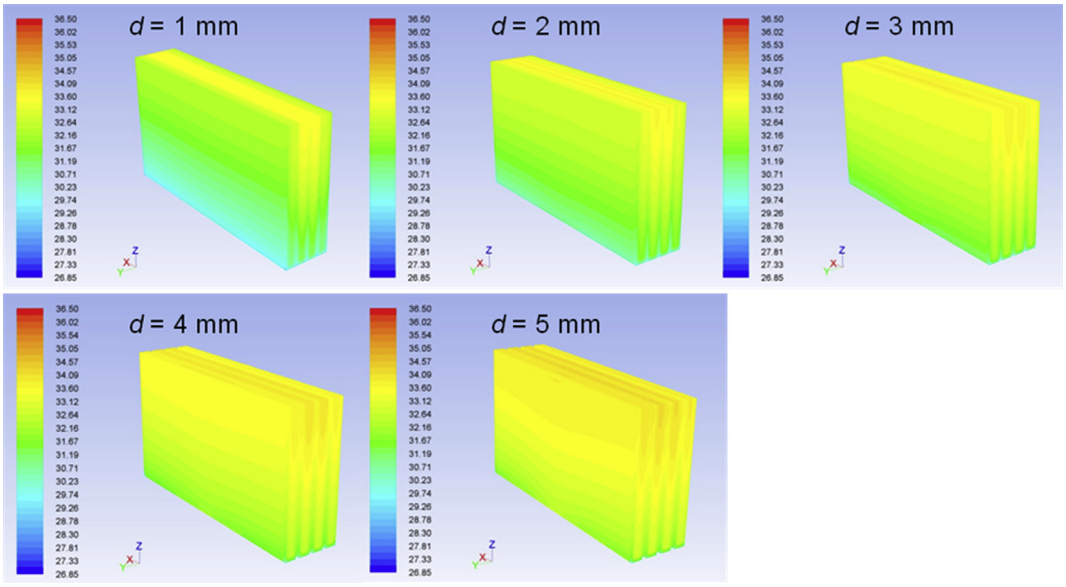

Fig. 12. Three-dimensional temperature distributions (unit: °C) within the cells after 600 s for one-side cooling design with various gap spacing values at $V = 20.4\ m^3\ h^{-1}$.

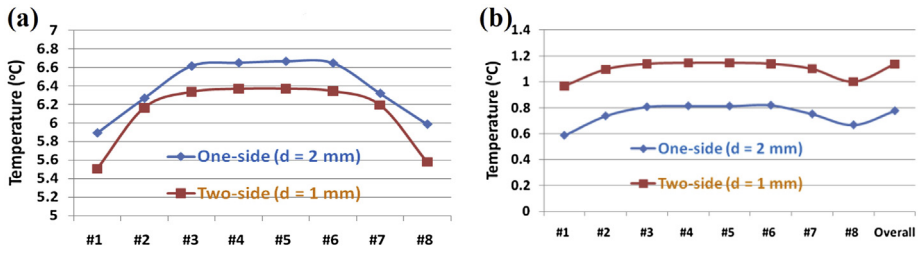

Fig. 13. The predicted (a) maximum temperature rise and (b) temperature uniformity parameter within individual cells for the case of one-side cooling with $d = 2$ mm in comparison to that of two-side cooling with $d = 1$ mm.

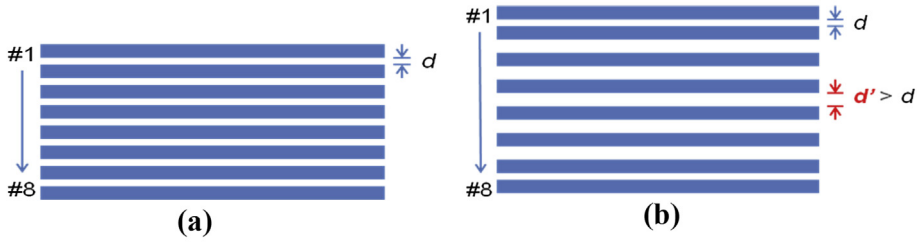

Fig. 14. Schematic diagram of the (a) original evenly-positioned design and the (b) proposed design of uneven gap spacings.

with the side cells being cooled more effectively. In order to moderate this problem of uneven cooling, uneven spacing of the gaps with a two-side cooling scheme was investigated next.

4.7. *Proposed design no. 2: exploring the uneven spacing of the gaps*

Because the side cells are generally cooled more effectively, the middle gaps can be somewhat widened to allow more cooling air flowing through these channels. This is expected to cool the cells in the middle of the module more effectively. This proposed design is shown schematically in Fig. 14 in comparison to the original design. The five middle gaps were widened to a value d', which is greater than d, while the four side gaps were kept unchanged at their original value of d. Theoretically, the spacing of each individual gap may be adjusted to provide uniformity of air flow rate and pressure value at the respective inlet ports. Keeping the spacing of the side gaps to be same as the evenly distributed design of $d = 2$ mm, the spacing of the middle gap was increased to 3, 2.5, and 2.3 mm. The

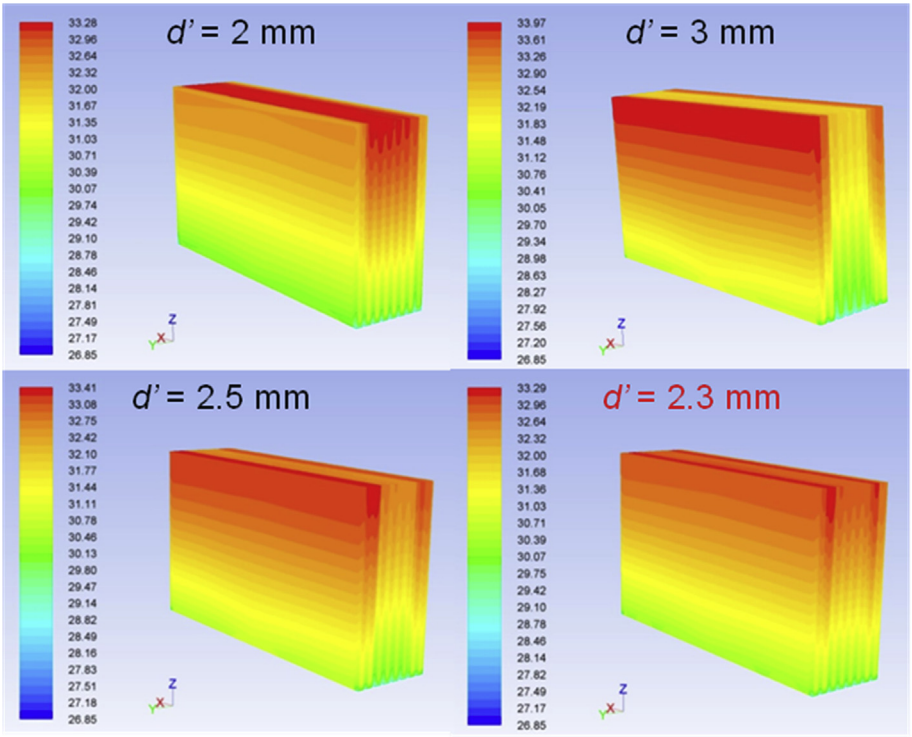

Fig. 15. The predicted three-dimensional temperature distributions (unit: °C) for different middle gap spacing values at $V = 20.4$ m^3 h^{-1}.

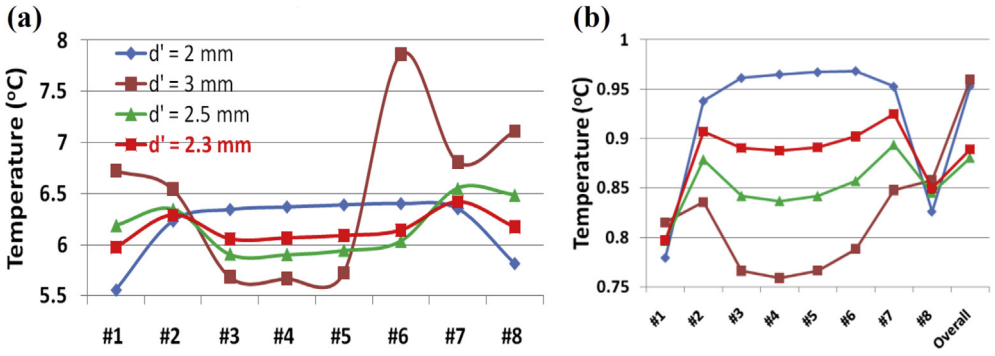

Fig. 16. The predicted (a) maximum temperature rise and (b) temperature uniformity for different values of the middle gap spacing at $V = 20.4\ m^3\ h^{-1}$.

flow rate of the fan was maintained at 20.4 $m^3\ h^{-1}$. The predicted three-dimensional temperature distributions in the cells for those gap spacing values are compared in Fig. 15.

It was observed that even though the temperature distributions were significantly affected by widening of the gap spacing in the middle of the module, the maximum temperature rise remained nearly constant. The widening of the gap spacing in the middle of the module to a proposed value of d' cannot be too excessive. For example, for a proposed gap spacing of $d' = 3$ mm, the middle cells are now cooled more effectively than the sides ones—the opposite of what prompted the proposed change. On the contrary, the gap spacing of $d' = 2.3$ mm exhibits nearly uniform cooling for all cells. In order to make concluding statements on the utility of uneven gap distances, quantitative data showing the predicted maximum temperature rise and temperature uniformity within individual cells are compared in Fig. 16. It is found that the proposed unevenly distributed design with a moderate gap spacing of $d' = 2.3$ or 2.5 mm provides a fairly uniform maximum temperature rise for each of the eight cells (Fig. 16a). Simultaneously, the proposed moderate widening of the gap from 2 mm to $d' = 2.3$ or 2.5 mm brings about improved temperature uniformity among the cells (Fig. 16b). In other words, the unevenly distributed design can lead to a more uniform cooling of the cells within the module. However, for these suggested changes in the spacing of the gaps, we did not come up with a temperature uniformity level common to all the cells.

5. Conclusions

The effects of gap spacing and air flow rate on cooling effectiveness of the existing air-cooled battery module have been examined and some concluding remarks can thus be drawn. Firstly, for the existing module with two-side cooling (on each side of each cell) and even spacing between the neighboring cells:

1. Without forced air cooling, the predicted temperature rise values are extremely close to those predicted by the simple lumped model, thus signifying the negligible role of natural convection.
2. With the air flow rate of the fan maintained constant, the maximum temperature rise always increases while the overall temperature uniformity is improved as the gap size is increased. For this arrangement, the side cells exhibited improved temperature uniformity in comparison to those in the middle of the module as the gap spacing was increased. This was shown to be due to the uneven distribution of the cooling air flowing between neighboring cells.
3. With a constant gap spacing, both the maximum temperature rise and the overall temperature uniformity decrease as the air flow rate of the fan is raised. The side cells exhibited improved temperature uniformity in comparison to those in the middle of the module as the air flow rate was increased. Again, this was shown to be due to the uneven distribution of the cooling air flowing between the neighboring cells.

Secondly, considering the 20 combinations of gap spacing and air flow rates of the fan for the existing arrangement:

4. Reducing the gap and/or increasing the flow rate of the fan led to a decrease of the maximum temperature rise of the module. On the other hand, to realize better temperature uniformity over the module, the gap spacing should be of a moderate length.
5. For the highest gap spacing ($d = 4$ and 5 mm), the vertical temperature gradients are significantly suppressed but the discrepancies among cells become more marked. Side cell #1, which is farthest from the fan, always exhibits the best temperature uniformity and the lowest temperature rise as compared to the other cells.
6. With low flow rates and narrower gap spacing, the cooling air was distributed more evenly among the gaps, which in turn affects the maximum temperature rise and the uniformity of the temperature distribution. Operating with $d = 3$ mm and $V = 40.8\ m^3\ h^{-1}$ appears to be the best choice that satisfies the trade-off requirements of the fan power, maximum temperature rise, and temperature uniformity of the existing module.

Thirdly, exploring alternative designs to evaluate schemes with one-side cooling and uneven gap spacing:

7. Using the same gap spacing and blower flow rate, one-side cooling is less effective than two-side cooling. However, the compensation is that the entire module is more compact by using one-side cooling. If the volume of the module is fixed, the one-side cooling scheme exhibits slightly higher temperature rises for each cell, but has more uniform temperature.
8. Uneven gap spacing affects the temperature distributions, but did not impact the maximum temperature rise of the module significantly. On the other hand, moderate widening of the gaps improves the temperature uniformity among the cells.

Considering the variety of the design change options that were explored, namely one-side vs. two-side, uneven vs. even gap spacing and their combinations within the framework of the existing thermal management scheme, it is concluded that the temperature gradients along the air flow direction can be affected but are generally unavoidable. To address the unavoidable problem of non-uniform temperature fields within each individual cell

of the existing air-cooled design, suggested future work may consider:

1. Filling the air gaps with highly conductive extended surfaces. The utilization of extended surfaces is expected to enhance the heat transfer rates between the cell surfaces and the cooling air flow.
2. Filling the air gaps with phase change materials, as proposed by Al Hallaj and Selman [22]. The constant-temperature operation of phase change materials will be an ideal approach in this application.

Disclaimer

This report was prepared as an account of work sponsored by an agency of the United States Government. Neither the United States Government nor any agency thereof, nor any of their employees makes any warranty, express or implied, or assumes any legal liability or responsibility for the accuracy, completeness, or usefulness of any information, apparatus, product, or process disclosed, or represents that its use would not infringe privately owned rights. Reference herein to any specific commercial product, process, or service by trade name, trademark, manufacturer, or otherwise does not necessarily constitute or imply its endorsement, recommendation, or favoring by the United States Government or any agency thereof. The views and opinions of authors expressed herein do not necessarily state or reflect those of the United States Government or any agency thereof.

Acknowledgment

This material is based upon work supported by the National Renewable Energy Laboratory (a Department of Energy national laboratory) under Subcontract No., LGC-9-99147-01 (DOE Prime Contract Number DE-AC36-08GO28308).

References

[1] A.A. Pesaran, Battery thermal management in evs and hevs: issues and solutions, in: Advanced Automotive Battery Conference, Las Vegas, NV, February 6–8, 2001, p. 10.
[2] A. Vlahinos, K. Kelly, J. Rugh, A. Pesaran, Improving battery thermal management using design for six sigma process, in: 20th Electric Vehicle Symposium, Long Beach, CA, November 15–18, 2003, p. 14.
[3] S. Al Hallaj, H. Maleki, J.S. Hong, J.R. Selman, Journal of Power Sources 83 (1999) 1–8.
[4] N. Sato, Journal of Power Sources 99 (2001) 70–77.
[5] S. Al Hallaj, J.R. Selman, Journal of Power Sources 110 (2002) 341–348.
[6] Y. Chen, J.W. Evans, Journal of The Electrochemical Society 140 (1993) 1833–1838.
[7] D. Brown, R.G. Landers, Journal of The Electrochemical Society 159 (2012) A2043–A2052.
[8] A.A. Pesaran, Journal of Power Sources 110 (2002) 377–382.
[9] P. Nelson, D. Dees, K. Amine, G. Henriksen, Journal of Power Sources 110 (2002) 349–356.
[10] V. Srinivasan, C.Y. Wang, Journal of The Electrochemical Society 150 (2003) A98–A106.
[11] V. Srinivasan, J. Newman, Journal of The Electrochemical Society 151 (2004) A1530–A1538.
[12] M. Verbrugge, B. Koch, Journal of The Electrochemical Society 153 (2006) A187–A201.
[13] K.A. Smith, C.D. Rahn, C.-Y. Wang, Energy Conversion and Management 48 (2007) 2565–2578.
[14] D. Dees, E. Gunen, D. Abraham, A. Jansen, J. Prakash, Journal of The Electrochemical Society 155 (2008) A603–A613.
[15] L. Cai, R.E. White, Journal of The Electrochemical Society 156 (2009) A154–A161.
[16] G.H. Kim, K. Smith, K.J. Lee, S. Santhanagopalan, A. Pesaran, Journal of The Electrochemical Society 158 (2011) A955–A969.
[17] K. Smith, C.-Y. Wang, Journal of Power Sources 160 (2006) 662–673.
[18] G.H. Kim, A. Pesaran, Battery thermal management system design modeling, in: 22nd International Battery, Hybrid and Fuel Cell Electric Vehicle Conference, Yokohama, Japan, October 23–28, 2006, p. 16.
[19] R. Mahamud, C. Park, Journal of Power Sources 196 (2011) 5685–5696.
[20] A. Pesaran, T. Markel, H.S. Tataria, D. Howell, Battery requirements for plug-in hybrid electric vehicles: analysis and rationale, in: 23rd International Electric Vehicles Symposium and Exposition, Anaheim, CA, December 2–5, 2007, p. 14.
[21] EPA US06 or Supplemental Federal Test Procedure (SFTP), Available from: http://www.epa.gov/otaq/standards/light-duty/sc06-sftp.htm, retrieved Februrary 16, 2013.
[22] S. Al Hallaj, J.R. Selman, Journal of The Electrochemical Society 147 (2000) 3231–3236.